

**THE TRANSPORT AND FATE OF HELIUM IN MARTENSITIC STEELS AT FUSION RELEVANT HE/DPA RATIOS AND DPA RATES**—R. J. Kurtz (Pacific Northwest National Laboratory\*), G. R. Odette, T. Yamamoto (University of California, Santa Barbara), D. S. Gelles (Pacific Northwest National Laboratory), P. Miao (University of California, Santa Barbara), and B. M. Oliver (Pacific Northwest National Laboratory)

Extended abstract of a paper submitted to the Journal of Nuclear Materials as part of the proceedings of the 12<sup>th</sup> International Conference on Fusion Reactor Materials, Santa Barbara, California, December 4–9, 2005.

### Experimental Procedure

The HFIR JP26 irradiation experiment contained a series of transmission electron microscopy (TEM) disks intended to study helium effects in ferritic/martensitic steels [1,2]. Table 1 lists specimens from that experiment chosen for examination. The Eurofer-97 disks were prepared with thin NiAl coatings so that irradiation would produce He by transmutation of the Ni and deposit that He uniformly in a thin layer ~ 6 to 8  $\mu\text{m}$  thick adjacent to the coating. Yamamoto et al. [3] give details of the specimen design and preparation. Following irradiation, samples were prepared for TEM using a cross-section technique to show He effects in the implanted layer near the NiAl coating. The procedure involved mounting the TEM disk between two half cylinders of Cu wire with thermal setting epoxy and slicing the composite wire using a slow speed saw equipped with a diamond-impregnated blade to produce 3 mm disks, with the TEM slice supported between the half-cylinders of Cu. Each composite disk was then dimple ground to a central thickness of ~ 100  $\mu\text{m}$ , and ion milled using a Gatan Precision Ion Polishing System. Ion milling was performed with 5 KV Ar ions to perforation so that the hole grew into the area of interest, followed by ion polishing at 2 KV for up to 1800 s to minimize Ar ion damage near the surface. Microstructural examinations were performed on a JEOL 2010F operating at 200 KeV in transmission with images recorded digitally.

Table 1. Summary of the NiAl coated Eurofer-97 transmission electron microscope discs irradiated in the JP26 experiment. Bold italic specimen numbers denote the samples examined in this study. The He concentrations are expected values based on pre-test calculations.

Nominal NiAl Thick., $\mu\text{m}$	300°C, 3.9 dpa		400°C, 3.9 dpa		500°C, 9 dpa	
	Spec. Nos.	[He], appm	Spec. Nos.	[He], appm	Spec. Nos.	[He], appm
0	R00, R01	0, 0	R10, R11	0, 0	R20, R21	0, 0
1	R02, R03	25, 23	R12, R13	24, 24	R22, R23	98, 98
2	R04, R05	41, 40	R14, R15	40, 40	R24, <b>R25</b>	167, 169
4	<b>R06</b> , R07	89, 82	<b>R16</b> , R17	82, 81	R26, <b>R27</b>	338, 372

Representative regions in the TEM images were selected for detailed analysis to determine the He bubble number densities and size distributions. Stereo pair images at ~ 500 nm underfocus were acquired so that the bubbles appeared white with a black outer ring. Foil thickness was measured from stereo pairs using a Hilger-Watts viewer for the center of each region analyzed. A square area centered on the thickness measurement location was analyzed for each specimen. The area analyzed was 0.05304, 0.1380, and 0.003812  $\mu\text{m}^2$  for specimens R16, R27, and R06, respectively. Grayscale TEM images were converted to black and white images, taking care not to change the shape or size of the bubbles during the conversion. Bubbles appear white against a black background in the converted images. A public domain software package was used to determine bubble area. Bubble diameters and size distributions were calculated from the area measurements assuming spherical bubbles.

\*Pacific Northwest National Laboratory (PNNL) is operated for the U.S. Department of Energy by Battelle Memorial Institute under contract DE-AC06-76RLO-1830.

The He concentration was measured in two samples taken from specimen R25. One sample was abrasively polished to remove only the NiAl coating, and the other was abrasively polished to remove both the NiAl coating and enough of the Eurofer-97 to leave only the He implanted layer. Prior to analysis, each of these pieces was cut in half using a small wire cutter, then rinsed in acetone, and air-dried. The mass of each specimen was determined using a calibrated microbalance traceable to the National Institute of Standards and Technology. Mass uncertainty is estimated to be  $\pm 0.001$  mg.

The He content of each specimen was determined by isotope-dilution gas mass spectrometry following vaporization in a resistance-heated graphite crucible [4]. The absolute amount of  $^4\text{He}$  released was measured relative to a known quantity of added  $^3\text{He}$  “spike.” The  $^3\text{He}$  spike was obtained by expanding and partitioning a known quantity of gas through a succession of calibrated volumes [5]. The mass spectrometer was calibrated for mass sensitivity during each series of runs by analyzing known mixtures of  $^3\text{He}$  and  $^4\text{He}$ .

## Results

Figure 1 gives TEM images showing the microstructure in the He implanted layer for specimen R06. This specimen was irradiated at  $300^\circ\text{C}$  to a dose of 3.9 dpa with a nominal  $4\ \mu\text{m}$  layer of NiAl. The expected implanted He concentration for this specimen is  $\sim 89$  appm as shown in Table 1. The underfocus imaging conditions in Fig. 1a were selected to enhance bubble contrast to aid identification and measurement. In Fig. 1b, dislocation contrast imaging conditions were employed to determine if He bubbles are preferentially associated with dislocations. Detailed bubble size and number density analysis reveals that the mean bubble diameter is  $\sim 0.9$  nm with a standard deviation ( $1\sigma$ ) of 0.2 nm. The measured bubble number density is  $\sim 3.6 \times 10^{23}\ \text{m}^{-3}$ . It should be noted the foil thickness measurement for R06 is uncertain. The value reported here is an average of the values for R16 and R27. Due to the very small sizes of the “black spot” defects produced at  $300^\circ\text{C}$ , it was difficult to determine the precise character of these defects. It is presumed they are small dislocation loops. The distribution of defects in Fig. 1b suggests that loop and/or void formation at  $300^\circ\text{C}$  may have been suppressed by the formation of a high-density of small He bubbles or clusters that served as point defect recombination centers. To explore this possibility the microstructure in the He implanted zone was compared to the microstructure in a He free region of the same specimen, see Figs. 2a and 2b. While the images in Figs. 2a and 2b were taken at different magnifications there was an indication that loop formation was suppressed in the He implanted zone. This indication needs to be further confirmed.

The bubble and dislocation microstructures observed in specimen R16 are presented in Figs. 3a and 3b, respectively. This specimen was irradiated at  $400^\circ\text{C}$  to a dose of 3.9 dpa. Similar to R06, the expected concentration of He in the implanted layer was  $\sim 82$  appm. It is clear that much larger bubbles, at significantly lower number density, form at this temperature compared to  $300^\circ\text{C}$ . The mean bubble diameter is 3.0 nm with a standard deviation of 1.4 nm. This is roughly three times larger than at  $300^\circ\text{C}$  with a larger dispersion in bubble sizes. In addition, the bubble number density is  $1.2 \times 10^{22}\ \text{m}^{-3}$  which is about 30 times smaller than at  $300^\circ\text{C}$ . Dislocation loops of both  $a/2\langle 111 \rangle$  and  $a\langle 100 \rangle$  character were produced at  $400^\circ\text{C}$ . Careful examination of Fig. 3b suggests that He bubbles nucleated on pre-existing dislocations.

Figures 4a and 4b illustrate the bubble and dislocation microstructures found in specimen R27 irradiated at  $500^\circ\text{C}$ . This specimen received a dose of 9 dpa, consequently the expected He concentration is 372 appm. The largest He bubbles were observed at this irradiation temperature. The mean bubble diameter is 4.3 nm with a standard deviation of 1.6 nm. The mean bubble diameter increased more than 40% relative to R16, but the dispersion of bubble sizes was approximately the same. Bubble number density is slightly larger than for R16 at  $1.5 \times 10^{22}\ \text{m}^{-3}$ . While more than four times as much He was injected into this specimen compared to R06 and R16, the main effect was to increase bubble size rather than increase the number density. It is evident from Figs. 4a and 4b that bubbles are associated with

dislocations. The “pearls-on-a-string” spatial arrangements of bubbles clearly follow the pre-existing dislocation pattern.

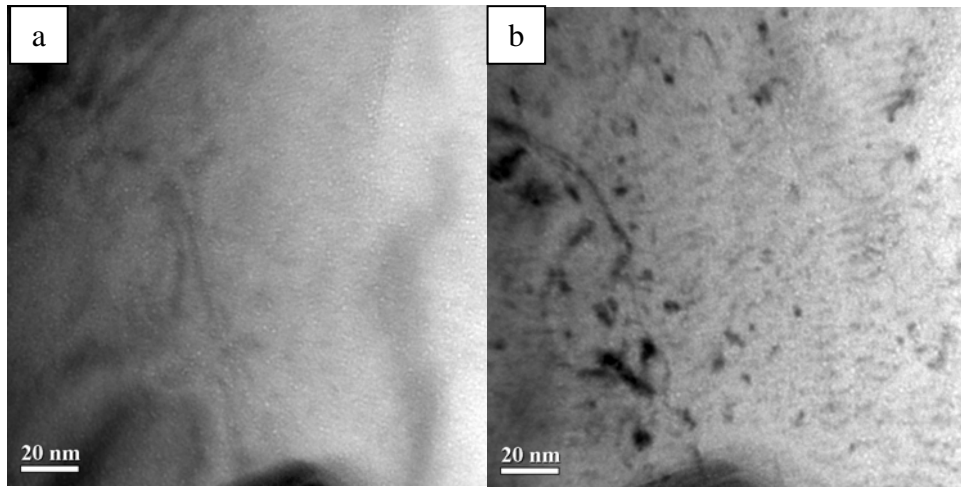


Fig. 1. TEM image showing a) the bubble microstructure and b) the dislocation microstructure for specimen R06 coated with 4  $\mu\text{m}$  of NiAl and irradiated at 300°C to a dose of 3.9 dpa. The expected He concentration is 89 apm.

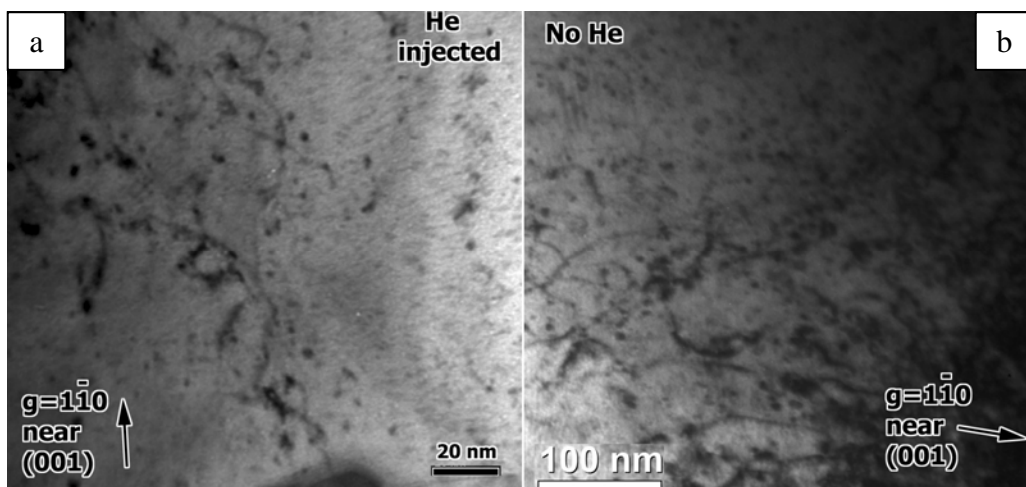


Fig. 2. TEM image showing the dislocation microstructures in specimen R06 in a) the He injected region near the NiAl coating and b) a region with no He injection far from the NiAl coating.

The results of the He measurements are given in Table 2 and are listed as total atoms of  $^4\text{He}$  released and as  $^4\text{He}$  concentrations in atomic parts per million ( $10^{-6}$  atom fraction). In Table 3, the samples consisting of only the He implanted layers are identified as R25A,B-thin and samples consisting of the full thickness TEM disc less the NiAl coating are designated as R25C,D-thick. Conversion from total He to He concentration was based on a calculated value of  $1.07 \times 10^{22}$  atoms/gram for Eurofer-97. It should be noted that this value, and the He concentrations obtained using it, are not very sensitive to small changes in material composition.

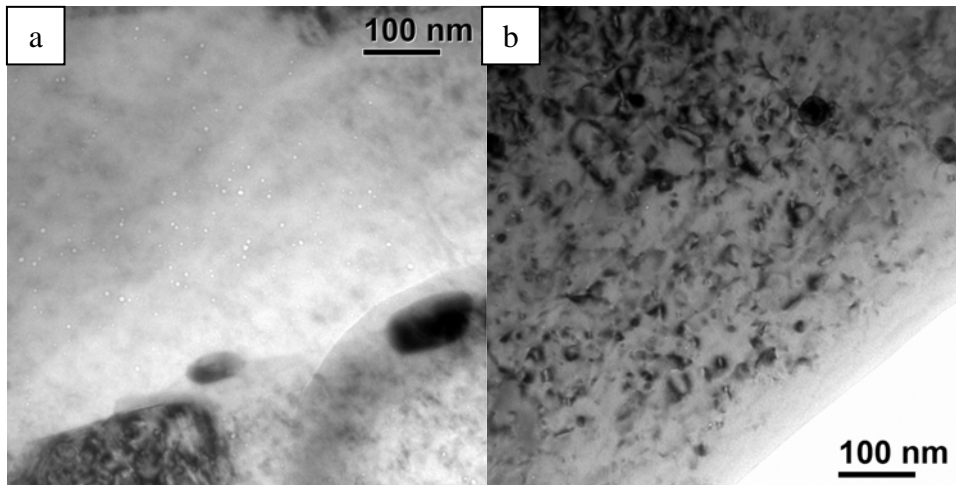


Fig. 3. TEM image showing a) the bubble microstructure and b) the dislocation microstructure for specimen R16 coated with 4  $\mu\text{m}$  of NiAl and irradiated at 400°C to a dose of 3.9 dpa. The expected He concentration is 82 appm.

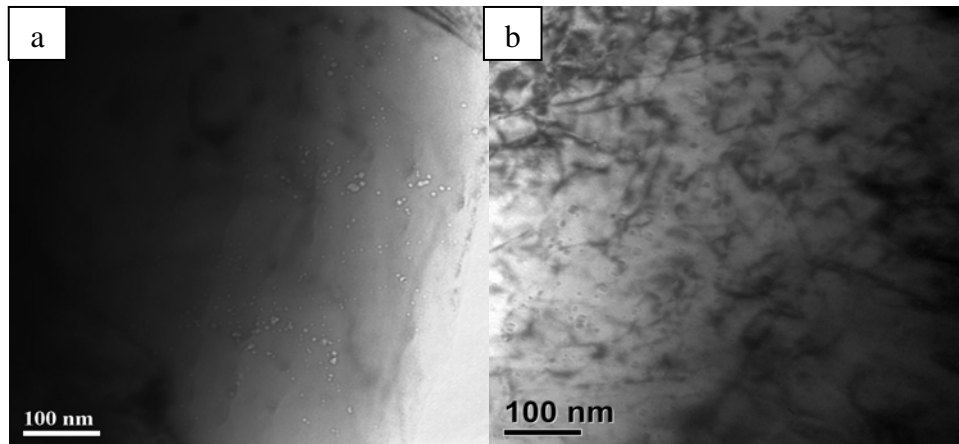


Fig. 4. TEM image showing a) the bubble microstructure and b) the dislocation microstructure for specimen R27 coated with 4  $\mu\text{m}$  of NiAl and irradiated at 500°C to a dose of 9 dpa. The expected He concentration is 372 appm.

Table 2. The He concentration in R25 measured by a high-sensitivity isotope-dilution magnetic sector mass spectrometer. Specimens denoted as “thin” were prepared by sanding away the NiAl layer and enough of the Eurofer-97 to leave only the He implanted layer. Specimens denoted as “thick” were prepared by removing only the NiAl layer leaving both the implanted and unimplanted Eurofer-97.

Specimen ID	Mass <sup>a</sup> , mg	Measured <sup>4</sup> He, 10 <sup>14</sup> atoms	He Concentration, appm <sup>b</sup>	
			Measured	Average <sup>c</sup>
R25A-thin	0.013	0.184	132	132 ± 0.0
R25B-thin	0.022	0.310	132	
R25C-thick	1.138	1.556	12.8	12.2 ± 0.9
R25D-thick	1.127	1.395	11.6	

<sup>a</sup>Mass of specimen for analysis. Mass uncertainty is ± 0.001 mg.

<sup>b</sup>Helium concentration in atomic parts per million (10<sup>-6</sup> atom fraction) with respect to the total number of atoms in the specimen.

<sup>c</sup>Mean and standard deviation (1 $\sigma$ ) of duplicate analyses.

Table 3. Measured He bubble sizes and number densities. He concentration calculated from the mean bubble radii and number densities. Note the MA957 specimen was examined in a companion study and included here for comparison to the Eurofer-97 results [3].

Specimen No.	Temp., °C	Foil thickness, nm	Mean bubble diameter, nm	Number density, m <sup>-3</sup>	Calc. He conc., appm
R06	300	150*	0.9 ± 0.2	3.6x10 <sup>23</sup>	270
R16	400	130	3.0 ± 1.4	1.2x10 <sup>22</sup>	128
R27	500	170	4.3 ± 1.6	1.5x10 <sup>22</sup>	384
MA957	500	52	0.6 ± 0.3	6.6x10 <sup>23</sup>	131

\*Foil thickness measurement is uncertain. The reported value is an average of the measurements for R16 and R27.

Mean He contents in the two samples were 132 appm for the thin specimens and 12.2 appm for the thick specimens. The 132 appm value is reasonably close to that calculated for the experiment (see Table 1). The lower He content in the thick samples represents dilution by the much lower He levels in the bulk material away from the implanted layer.

Absolute uncertainty (1 $\sigma$ ) in the individual He atom results, determined from the cumulative uncertainties the isotope ratio measurement, and the spike size, is estimated to be ~ 1%. For the He concentrations, the sample mass normally contributes negligibly to the final uncertainty. However, for the thin specimens, additional mass uncertainty of ~ 6% is present due to the very small sample size. The estimated uncertainties are consistent with the variability observed in duplicate analyses.

## Discussion

As summarized in Table 3, the mean bubble diameter increased systematically with increasing irradiation temperature, and the bubble density at 400 and 500°C was about 25 times smaller than at 300°C. Measurements of the He concentration in R25 correlate well with the concentration expected from pretest calculations (132 appm measured versus 169 appm predicted). Measurement of the He concentration in a full-thickness specimen that includes both the He injected zone and the He free region corroborate this result.

We recognize that the minimum bubble sizes observed are near the TEM resolution limit, so the precise nature of the bubble size distribution is uncertain below that limit. In addition, further work is needed to confirm that specimen preparation procedures, or the presence of surface oxides did not influence our measurements. To provide additional confidence in our results we calculated the He concentration in the

injected layer based on the measured average bubble sizes and number densities. We assume that all bubbles were in equilibrium at the irradiation temperature and that the bubble pressure,  $P$ , is given by:

$$P = \frac{2\gamma}{\langle r \rangle} \quad (1)$$

where  $\gamma$  is the surface energy, which is taken to be  $\sim 2 \text{ J/m}^2$ , and  $\langle r \rangle$  is the mean bubble radius. A high-pressure equation-of-state [6] was used to determine the mole fraction of He in bubbles at pressure  $P$ . We also assume that all of the injected He is contained in the visible bubble population. The estimated He concentrations for R06, R16, and R27 are 270, 128, and 384 appm, respectively (see Table 3). Recall that the expected He levels are 89, 82, and 372 appm. Except for R06, the estimated He concentrations based on the measured bubble sizes and number densities agree very well with expected levels. Uncertainty in the foil thickness estimate for R06, coupled with the difficulty of accurately determining the mean bubble size and number density for the very small bubbles in R06, are likely responsible for the difference between the estimated He concentration and the expected value.

An objective of our research is to develop and test models of He trapping in ferritic alloys in order to design microstructures with optimal resistance to dimensional instabilities and mechanical property degradation due to He. It is informative to compare the efficiency of He trapping in a nanostructured ferritic alloy such as MA957 with a conventional RAFM alloy such as Eurofer-97. In a companion study to the present work [3], NiAl coatings were applied to TEM discs of MA957 and irradiated under the same conditions as R27. The measured bubble sizes and number densities for the MA957 specimen are included in Table 2 for comparison with the Eurofer-97 results. While the measured mean bubble size is below the TEM resolution limit, and therefore uncertain, the MA957 results clearly illustrate that a high-density of nano-scale Y-Ti-O particles effectively trapped He and dramatically suppressed bubble growth. Indeed, the measured bubble density is on the same order as the Y-Ti-O particle density. Considering the uncertainty in the bubble size and density measurements for the MA957 specimen, the calculated He concentration is in remarkable agreement with the expected value (see Table 3).

## Conclusions

The He implanter layer concept has been demonstrated to be an effective experimental tool for producing controlled He-to-dpa ratios in Eurofer-97 TEM discs under neutron irradiation. Helium bubbles were found in the implanted region, adjacent to the NiAl layer, at all three irradiation temperatures, with estimated mean diameters of  $\sim 0.9$ ,  $3.0$ , and  $4.3 \text{ nm}$  at  $300$ ,  $400$ , and  $500^\circ\text{C}$ , respectively. In addition, at  $500^\circ\text{C}$ ,  $10 \text{ nm}$  faceted cavities were also observed, which may be voids. Minimum bubble sizes were near the TEM resolution limit for the specimen irradiated at  $300^\circ\text{C}$ . Loop and void formation at  $300^\circ\text{C}$  may have been suppressed by a high-density of small He bubbles serving as point defect recombination centers. At  $400$  and  $500^\circ\text{C}$ , pre-existing dislocations appear to be preferred He bubble nucleation sites. The addition of a high-density of nano-scale Y-Ti-O particles to a ferritic matrix effectively trapped He atoms and suppressed bubble growth. Additional work is needed to confirm that specimen preparation procedures or surface oxides did not influence these results.

## References

- [1] R. E. Stoller and H. Tanigawa, "Planning of the US-Japan JP-26 Experiment for Irradiation in the HFIR," Fusion Materials Semiannual Progress Report for Period Ending June 30, 2003, DOE/ER-0313/34 (2003) 142.
- [2] K. R. Thoms, D. W. Heatherly, S. H. Kim, R. G. Sitterson, and R. E. Stoller, "Assembly of the US-Japan JP-26 Experiment and Start of Irradiation in the HFIR," Fusion Materials Semiannual Progress Report for Period Ending December 31, 2003, DOE/ER-0313/35 (2004) 250.
- [3] T. Yamamoto, G. R. Odette, N. Hashimoto, D. T. Hoelzer, and H. Tanigawa, "The Transport and Fate of Helium in Nanostructured Ferritic Alloys at Fusion Relevant He/dpa Ratios and dpa Rates," Journal of Nuclear Materials (submitted).
- [4] H. Farrar and B. M. Oliver, "A Mass Spectrometer System to Determine Very Low Levels of Helium in

Small Solid and Liquid Samples," J. Vac. Sci. Technol. A4 (1986) 1740.

[5] B. M. Oliver, J. G. Bradley, and H. Farrar, "Helium Concentration in the Earth's Lower Atmosphere," Geochim. Cosmochim. Acta 48 (1984) 1759.

[6] R. E. Stoller and G. R. Odette, "Analytical Solutions for Helium Bubble Parameters Using a Hard Sphere Equation of State," J. Nucl. Mater. 131 (1985) 118.